Automatic Earthquake Detection and Phase Picking in Muong Te, Lai Chau Region: An Application of Machine Learning in Observational Seismology in Vietnam

Abstract

We applied the automatic detection and picking of P- and S-wave for one-year continuous raw seismic data from 17 seismic stations in the Muong Te area, northwestern Vietnam. The deep learning picker, Earthquake Transformer, has performed automatically picking of both P- and S-wave, phase association and we located the earthquakes by using HYPOINVERSE and NONLINLOC programs. The newly derived catalog consists of 893 events, which is approximately 13 times the number of events in the manual catalog. From this new catalog, we can observe more earthquakes related to the Muong Te M_L 4.9 earthquake on June 16th, 2020, and the earthquake activity in the other faults such as the Dien Bien Phu and Muong Nhe faults. The extended catalog can be used for further study on the seismogenesis and seismic velocity structure of crust beneath northwestern Vietnam.

Keywords: Muong Te earthquake; Machine Learning; EQTranformer; Dien Bien Phu fault; Upstream Da River fault; Earthquake Monitoring

1. Introduction

In recent years, the rapid development of machine learning algorithms, especially neural network, and deep learning have allowed for new improvements in various fields of sciences. Recent advances in machine learning algorithms have also been applied to the seismological aspects as

outlined by Kong et al. (2019). Among various applications of neural networks and deep learning, automatic earthquake detection and phase picking is the major problem in modern seismology, which currently attracts attention from seismologists. The earthquake detection and phase picking can be considered as one of the very first subjects of seismology study since digital seismometers were used, with the first algorithm was the well-known short-term average/ long-term average (STA/LTA) method (Allen, 1978). This algorithm is still widely used currently due to its effectiveness and is easy to apply for seismic data compare to other methods (Trnkoczy, 2009). Other traditional pickers follow a similar approach to detect earthquakes: define a function to represent the features of coming earthquake signals and use a preexisting threshold to detect and pick the phase (Baer and Kradolfer, 1987; Baillard et al., 2014; Cichowicz, 1993; Saragiotis et al., 2002; Sleeman and Van Eck, 1999). Contrasting to these methods, the machine learning pickers, which use deep learning in the algorithm, do not define a specific function but rely on the "training" process from a large amount of data, i.e., hundreds of thousands to millions of waveforms. The three notable deep learning pickers are general phase generalized seismic phase detection (GPD) (Ross et al., 2018), PhaseNet (Zhu and Beroza, 2019), and the current state-of-the-art Earthquake Transformer (EQT) (Mousavi et al., 2020). These deep-learning-based pickers have improved the quantity and quality of earthquake detection and phase picks in various studies (Hutchinson et al., 2021; Liberty et al., 2021; Liu et al., 2020; Wang et al., 2020; Xiao et al., 2021; Zhou et al., 2021). Moreover, a new study on evaluating the performance of the deep learning pickers has indicated the Earthquake Transformer can be considered as the most reliable picker for local earthquakes within the epicentral distance of about 350 km (Münchmeyer et al., 2021). In addition to machine learning picker using global dataset, a neural-network based picker was developed by using the

local seismic data in Lai Chau area, northwestern Vietnam, however, due to the small number of events, the model shows a quite low true positive accuracy (Wiszniowski et al., 2021).

On 16 June 2020, a moderate-sized earthquake of local magnitude (M_L) 4.9 struck thoroughly the Muong Te area, where located in northwesternmost part of Vietnam. This is the strongest earthquake in Muong Te block over 100 years ago and has caused some damage to infrastructure and public panic in the area near the source (Fig. 1). This earthquake was preceded and followed by several foreshocks and aftershocks with magnitude greater than 1.0. The earthquake sequence was located close to the junction of the Upstream Da River fault, Muong Te fault, and several submeridian faults (Fig. 1). In Muong Te block, the most notable fault in the region is the N-S trending Dien Bien Phu fault which is considered as a boundary between Simao and Indochina blocks. In addition, the Muong Te region includes three other remarkable rank II faults including the Upstream Da River fault, Muong Te fault, and Muong Nhe fault (Nguyen et al., 2019). Due to the presence of these faults, a more completed earthquake catalog is needed to deepen the understanding of seismogenic fault zones in Muong Te block and adjacent areas.

In this study, we applied a deep-learning picker – EQT phase picker (Mousavi et al., 2020) to build up a more completed earthquake catalog in the Muong Te region. The picker was applied to continuous waveform data, and the phase picks were associated to form an event, follow by locating the event using traditional locating methods. The number of earthquakes in the new catalog has increased at least 13 times compared to the original catalog, which clearly revealed that the fault system was more active than previous findings. In a further study, the new catalog provides an opportunity to study more detail on the seismogenic structure, fault geometry, and seismic hazard assessment for northwestern Vietnam.

2. Data and Method

2.1. Data

2.1.1. Seismic data

We have collected the 3-component seismic waveforms from 17 seismic stations in the Muong Te area in the period from January to December 2020 (Fig. 1 and Table 1). Among these seismic stations, three stations are equipped with extremely short-period seismometers (CNUD, MMOD, MLAV), while the rest are equipped with broadband seismometers (MTE, MTE2, MLVB, CCA, NNA, NNU, MLVB, and stations start with "VN"). Most of the seismic stations are permanent or temporary deployed before the Muong Te earthquake, so they have operated for the whole experiment time, while station MTE2 was deployed after the earthquake by the Institute of Geophysics (IGP) – Vietnam Academy of Science and Technology. As described in (Mousavi et al., 2020), the EQT phase picker was built using data from various types of seismometers, including those used in our study, so the picker would be expected to work well with our data.

2.1.2. Earthquake catalog

Before this study, the IGP has monitored the seismicity in the region and compiled an earthquake catalog. The catalog was built by routine workflow consisting of three main steps: 1) earthquake detection, 2) manually phase picking and storing the data in SEISAN format (Havskov and Ottemoller, 1999), and 3) locating the earthquake using traditional locating methods, e. g. HYPOINVERSE (Klein, 2002) or HYPO71 (Lee and Lahr, 1972). The catalog consists of 67 events with local magnitudes (M_L) of $1.0 \leq M_L \leq 4.9$. To distinguish this catalog from the resulted earthquake catalog from this study, we named this catalog MTMAN while the new catalog was named MTEQT. To have an analysis on the use of the new method in making the earthquake catalog, it is necessary to compare between MTMAN and MTEQT in following criteria: the

number of earthquakes, the source parameters (location and original time) of the earthquakes which are in both catalogs, and the phase picks. These information and result of this comparison will be presented in the discussion part.

2.2. Method

2.2.1. The EQT picker

The EQT is a quite complicated deep learning model for earthquake detection and phase picking with great performance when apply to local earthquakes (Mousavi et al., 2020). The model was built using the STanford EArthquake Dataset (STEAD), which contains millions of labeled waveforms that recorded local earthquakes within about 300 km from various types of instruments (Mousavi et al., 2019). In this study, the network structure of the EQT model is summarized and simplified in Fig. 2, which includes a multilayer encoder and three distinct decoders. The encoder is used to transform the three-component waveforms into high-level data that the model can recognize while the decoders are used to extract the features and return the output. In this model, the output is expressed in the form of three distinct probabilities: earthquake detection, P-phase, and S-phase. Readers may refer to Ross et al. (2018), Zhu and Beroza (2019), and Mousavi et al. (2020) for further detailed explanations on how the neural network is designed to process the seismic waveform data. In short, the neural network used in these studies is inspired by the neural network commonly used in image processing, e.g., convolution neural network (CNN) (LeCun and Bengio, 1995), long short-term memory (LSTM) (Hochreiter and Schmidhuber, 1997) and transformer-attention (Vaswani et al., 2017) because, in computer science, three-component seismic waveforms (vertical and two horizontal components) can be processed similarly to RGB (red, green, blue) images.

The EQT is specialized in detecting and picking the local earthquakes, therefore is suitable for seismic waveforms recorded close to the earthquakes with the distance to the hypocenters of less than 300 km. The training data of the EQT model is STEAD dataset, in which the authors have used approximately 1 million earthquake waveforms and 300 thousand noise recorded by seismic stations with the variety of the source mechanisms, tectonic regions, focal depths, magnitude sizes, and seismic instrument types (Mousavi et al., 2019). 113 thousand test waveforms have been used to evaluate the detection ability of EQT phase picker, which resulted in 1 false positive and 0 false negatives. In addition, the model also showed very small differences in P- and S-phase picks compared to manual picking (Mousavi et al., 2020). Based on these results and characteristics, we chose the EQT model to detect and pick the seismic phase from the local seismic network in Muong Te area in one year for this study.

2.2.2. Data processing workflow

To apply the phase picker to detect Muong Te earthquakes, we followed a process illustrated in Fig. 3. The workflow includes 7 steps: 1) collect waveform data; 2) preprocessing; 3) divide the data into smaller sets (monthly data); 4) model parameter calibration; 5) automatic picking; 6) phase association and quality control; and 7) locate the earthquakes and build the catalog. We will briefly describe these steps in the following.

The first step is to collect the waveform data from 17 seismic stations in the period from January to December, 2020. We collected the 3-component seismic waveforms: the vertical component Z and two horizontal components N and E. To have maximum available data, all components in one station (BH*, EH*, and HH*) were collected.

The collected data was in the raw format without any processing, therefore we need to preprocess the data (Fig. 4). The preprocessing step includes 3 main techniques: bandpass filter set the sampling rate of 20 Hz and normalization. Figure 4a illustrates a one-day waveform before and after we applied a 2 Hz – 5 Hz bandpass filter. As shown in the figure, we can see the seismic signals have been enhanced and more phases can be observed. Figure 4b shows an example of the downsampling rate of a waveform from 100 Hz to 20 Hz, in general, the waveform does not show much difference after downsampling. However, this step is necessary to decrease the size of data and fit the criteria of the phase picker. Lastly, we normalized the waveform by demean (correct by the average value) and detrend (correct the trend of the data) techniques, thus the maximum and minimum value in the y-axis was changed (Fig. 4c). These techniques are very common and frequently used to process the seismic data.

After being preprocessed, all of the waveforms were cut into one-day files and grouped into subsets of one-month data. To choose the appropriate model parameter for the phase picker and check if the picker worked properly, we used a small number of data to do test runs. In this step, several one-day waveforms were chosen to be applied EQT picker and then we modified the model parameter accordingly. Compared to the traditional pickers, the model parameters in the deep learning model have less impact on the result. The calibrated parameters include overlap between two waveforms to prevent disruption of the data, detection threshold, and P- and S-phase picking threshold. These thresholds are the minimum probability that the model accepts whether the signal is earthquake or detected as P- or S-phase and are chosen to be between 0 and 1. After several trials runs, we selected the model parameters as shown in Table 2. These optimized parameters were similar to the suggestion from the model description (Mousavi et al., 2020), with an overlap of 0.2; an earthquake detection threshold of 0.1; and the P- and S-pick thresholds of 0.2.

The waveforms were then processed by the phase picker. In this step, the EQT model reads simultaneously 3-component waveforms and output the probability of earthquake detection, P-pick, and S-pick every 15 seconds. When a signal has a higher probability than the set threshold, the time of the seismic phase will be recorded and plotted in spectrogram images. Figure 5 shows examples of detected earthquakes, P- and S-phase pick with their corresponding spectrogram images.

The phase picks were then associated and grouped into events, which were consequently located by using traditional earthquake location methods: HYPOINVERSE (Klein, 2002) and NONLINLOC (Lomax et al., 2009). We also checked the quality of the phase picks and detection in this step by inspecting the visualization of phase picks, and the earthquake locations. Figure 6 illustrates the performance of earthquake detection on the day of the Muong Te earthquake (16/6/2020) for two stations CCA and VN04. Basically, the seismic signals have been identified accurately, we will present more analysis based on comparison with the original catalog MTMAN to exam the quality of the method. We also determined the local magnitude of newly earthquake catalog by applying the equation from Hutton and Boore (1987):

$$M_L = \log A_{W-A} + 1.11 \log_{10}(r) + 0.00189r - 2.09$$

In which, the $A_{W\text{-}A}$ is the Wood-Anderson zero-to-peak amplitude (mm) of the horizontal seismogram; r is the epicentral distance and M_L is the local magnitude of the event.

3. Result

3.1. Result of the earthquake detection and phase picking

After the automatic picking step and phase association, we have obtained a total of 1198 events with 4983 P picks and 4761 S picks. Figure 7 shows examples of phase picking for 2 events (the

Muong Te mainshock and an earthquake with M_L 2.5) after we have associated the phases. Fig. 7a, c shows a typical case of the earthquake in which the phases are quite clear to see. In this case, the picks obtained from automatic picking and manual picking are very close, with the different times of them in most stations being less than 0.5 second. On the other hand, Fig. 7b, d shows a case that is not detected in the manual catalog MTMAN, mostly due to the waveforms being very unclear with a high level of noise. In fact, for the case of the Muong Te earthquake, most of the earthquakes are quite small with magnitudes smaller than 4, therefore the signals are often weak and missed under manual processing while can be detected using the EQT. This proves that the automatic deep-learning picker is necessary and useful to extend the earthquake catalog.

The number of detections, which indicates the event detection for each station is plotted in Fig. 8. From the figure, we can observe 4 stations with high number of detections: NNU, CCA, NNA, and MTE, in which each station detects more than 8000 detections. These four stations are located quite close to the Muong Te earthquake, thus suggesting the high number of detections relating to the Muong Te earthquake sequence. This number of detections is much lower than the number of events due to a high number of detections that cannot be associated with other phases from other stations, thus preventing the formation of an event. The lower number of detections in other stations might be due to the further distance from the event, thus the signals would be too weak, the incomplete record of the data, and/or a high level of noise.

3.2. Result of earthquake location and catalog compilation

After locating the earthquake, we applied quality control of the earthquakes by rejecting duplicate events in which the original time and locations are close. Finally, we have obtained a total of 893 events with 3615 P phase and 3391 S-phase. The local magnitude of the earthquakes was also calculated in this part. The locations of the earthquakes from the new catalog are shown in Fig. 9a,

while Fig. 9b shows the locations of the earthquakes from the manual catalog for comparison. From the figure, we can see that most of the earthquakes located in the Muong Te earthquake source zone. Overall, most of the earthquakes occurred at a shallow depth between 5 to 20 km, which is not clear in the manual catalog. In the cross-section plot cutting perpendicular with the Upstream Da River fault, we can see that the earthquakes located concentrated near the fault.

Figure 10 shows the distribution of earthquakes with time in the new catalog. A significant increase in the number of earthquakes can be seen in 6/2020, which corresponds to the time of the Muong Te earthquake followed by a slight increase of event in 7/2020. In 6/2020, there were 181 events while there were 90 events in 7/2020, which are 2.5-times and 1.25 times of the average earthquakes per month (average 72 events per month). These data emphasize the increase in seismic activity related to the Muong Te earthquake.

4. Discussion

4.1. Comparison between automatic and manual catalog

We first discuss the comparison between the automatic catalog MTEQT and the manual catalog MTMAN on quantity and quality. First of all, the number of the events from automatic picking is approximately 13 times that in the manual catalog (893 events compared with 67 events), with the minimum local magnitude of -0.7 in MTEQT, while the minimum local magnitude of MTEQT is 1.0. Furthermore, the processing time using the EQT phase picker was much shortened compared to the manual way. The total processing time of the building catalog using the deep learning phase picker was estimated to be about one day, while the manual-processing time for 1-year data with 17 stations could probably take a month.

On the other hand, we compared the quality of picks between the two methods. Fig. 11 shows the histogram of time difference for the P and S-picks, respectively. In general, the result shows a great concordance, the average difference and standard deviation of P picks are 0.02 s and 0.18s, respectively, while the average difference and standard deviation of S picks are -0.04 s and 0.05 s. These measurements of picking quality are quite similar to those reported for the model in the EQT paper (Mousavi et al., 2020), which implies that the picker performance for our data is consistent with the data used to make the EQT picker.

4.2. Extended catalog reveals hidden earthquake

As we can see in Fig. 9 and discussion in 4.1., the number of earthquakes detected has significantly increased in the area of the Muong Te earthquake. The main reason for this increase in the number of events is the ability of the EQT model to detect small hidden earthquakes, which are very unclear to detect manually. Take Fig. 7b, d as an example, we can see that, before applying a bandpass filter, the waveform is very difficult to recognize as a seismic event. The improvement of the detection rate results demonstrated that the new MTEQT catalog provides a far more detailed picture of how seismicity evolves in Muong Te block in the year of 2020.

Another worth mentioning point is the earthquake occurrence of other faults in the study area. As shown in Fig. 9a, the epicenters concentrated almost near the Muong Te earthquake region and very few earthquakes were found outside the source zone in the manual catalog, while a high number of events were detected not only in the Muong Te earthquake area but also in other places in the automatic catalog (Fig. 9b). The small earthquakes below magnitude 2.0 are occurring more often, in which people cannot feel the shaking and instruments can hardly detect. The MTEQT catalog revealed the small earthquake activity in the study area, especially the connected or blind

faults that associate with the mainshock. This is suggesting that there can be the interactions between one earthquake to another (Brodsky, 2019; Ross et al., 2019).

4.3. Prospect study based on the extended catalog

In seismological studies and especially research about the seismic source, identification of earthquakes is the most important task. Using the deep-learning phase picker EQT, we have not only identified more events compared to manual picking but also save time and human resources on processing seismic data. On top of that, the high-quality phase picking can allow for a better constraint of earthquake locations using absolute locating methods (HYPOINVERSE, NONLINLOC). On the other hand, a more completed earthquake catalog is crucial on successfully applying relative earthquake relocation, HYPODD (Waldhauser, 2001) or GrowClust (Trugman and Shearer, 2017) because, in these methods, earthquakes are divided into clusters based on how close the distance between each event. More events in each cluster may contribute to better relocation while a single earthquake cannot be relocated. The relative relocation methods are very effective in tracing the fault from seismicity, which reveals the seismogenesis and quantifies the seismic hazards (Trugman and Shearer, 2017; Waldhauser and Schaff, 2008). The extended catalog in our study region with preliminary earthquake location can now be used to apply earthquake relocation, thus may provide a better constraint of the earthquake process and mechanism.

Another prospective study from our extended catalog is studying the structure in the Muong Te area, particularly applying seismic tomographic methods. We take travel time seismic tomography as an example, in this method, travel times from earthquake-seismic stations are used to invert the velocity structure of the region where ray paths cross (Zhao, 2015). Fig. 12 shows the crossing ray paths from earthquakes to the seismic stations in the two catalogs. In this figure, a significant

increase in the number of ray paths for both P- and S-wave in the MTEQT catalog allows for seismic tomographic studies for the Northwestern part of Vietnam. A worth mentioning point in the extended catalog is that the number of S-wave ray paths (3391 S-phase) is almost the same as with the P-wave ray path (3615 P phase). This can improve the resolution of S-wave tomography compared to seismic tomographic inversion based on manual picking because the number of S picks are often notably less than the number of P picks due to inevitable large errors in picking the S phase manually.

5. Conclusion

In this study, we have applied the deep-learning phase picker EQT on the 1-year seismic data from 17 seismic stations in the Muong Te region. The phase picks were then grouped as events and located using HYPOINVERSE and NONLINLOC, calculated for the local magnitude, and compiled into an extended catalog MTEQT. The new catalog consists of 893 events, which is 13 times compared to the manual catalog. This new method has allowed us for a more completed catalog with a dramatic increase in the number of phase picks and time-saving. This improved catalog has opened up for subsequent studies on the earthquake genesis and structure of the study area.

Acknowledgments.

This study has been funded by Vietnam Academy of Science and Technology (VAST) under grant number: CT0000.02/22-23 and Vietnam National Foundation for Science and Technology Development (NAFOSTED) under the grant number: 01/2021/ĐX.

FIGURE CAPTIONS

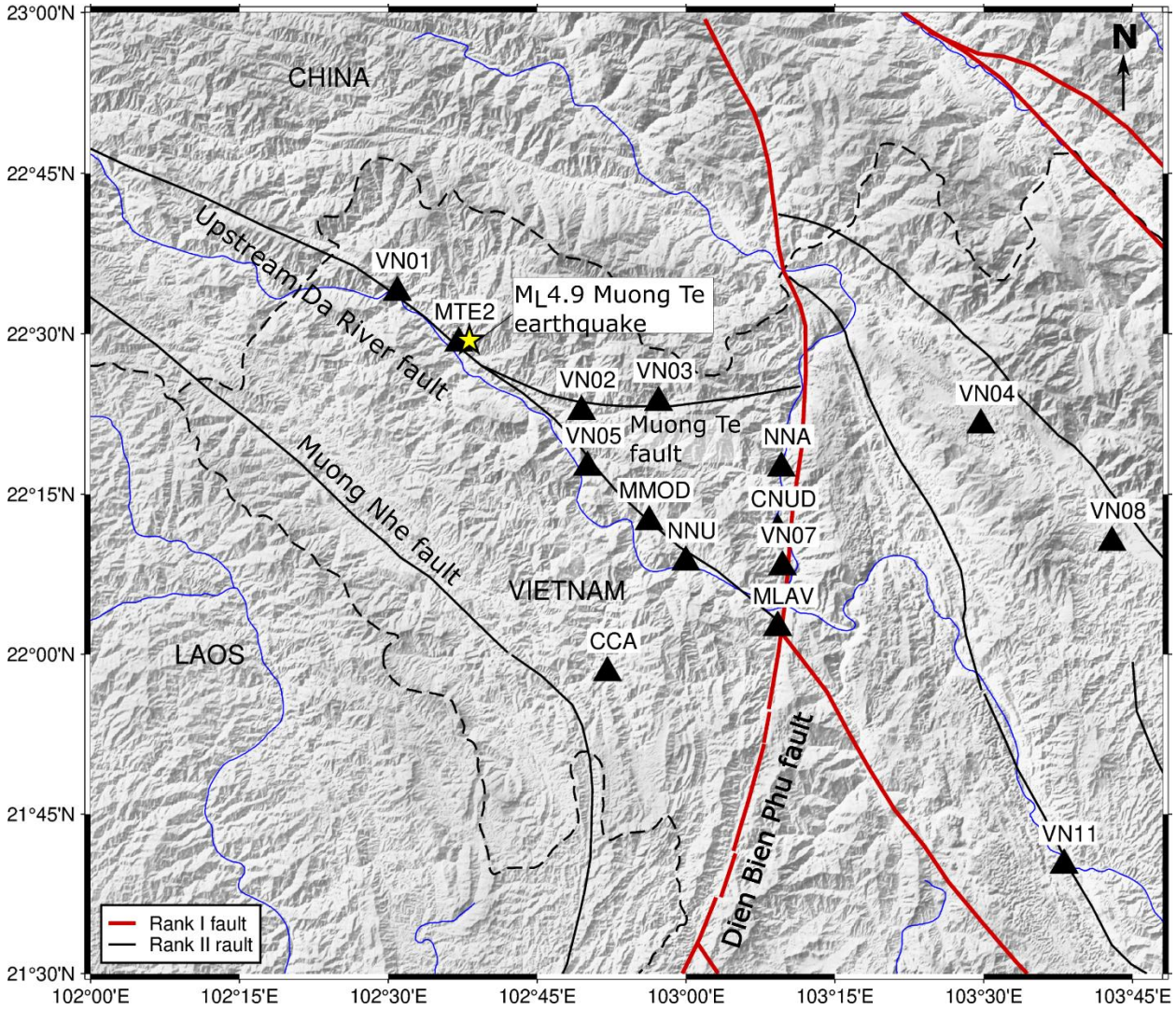

Figure 1. Map showing the study region; the faults and their ranks are from (Nguyen et al., 2019); black triangles indicate the seismic stations used in this study.

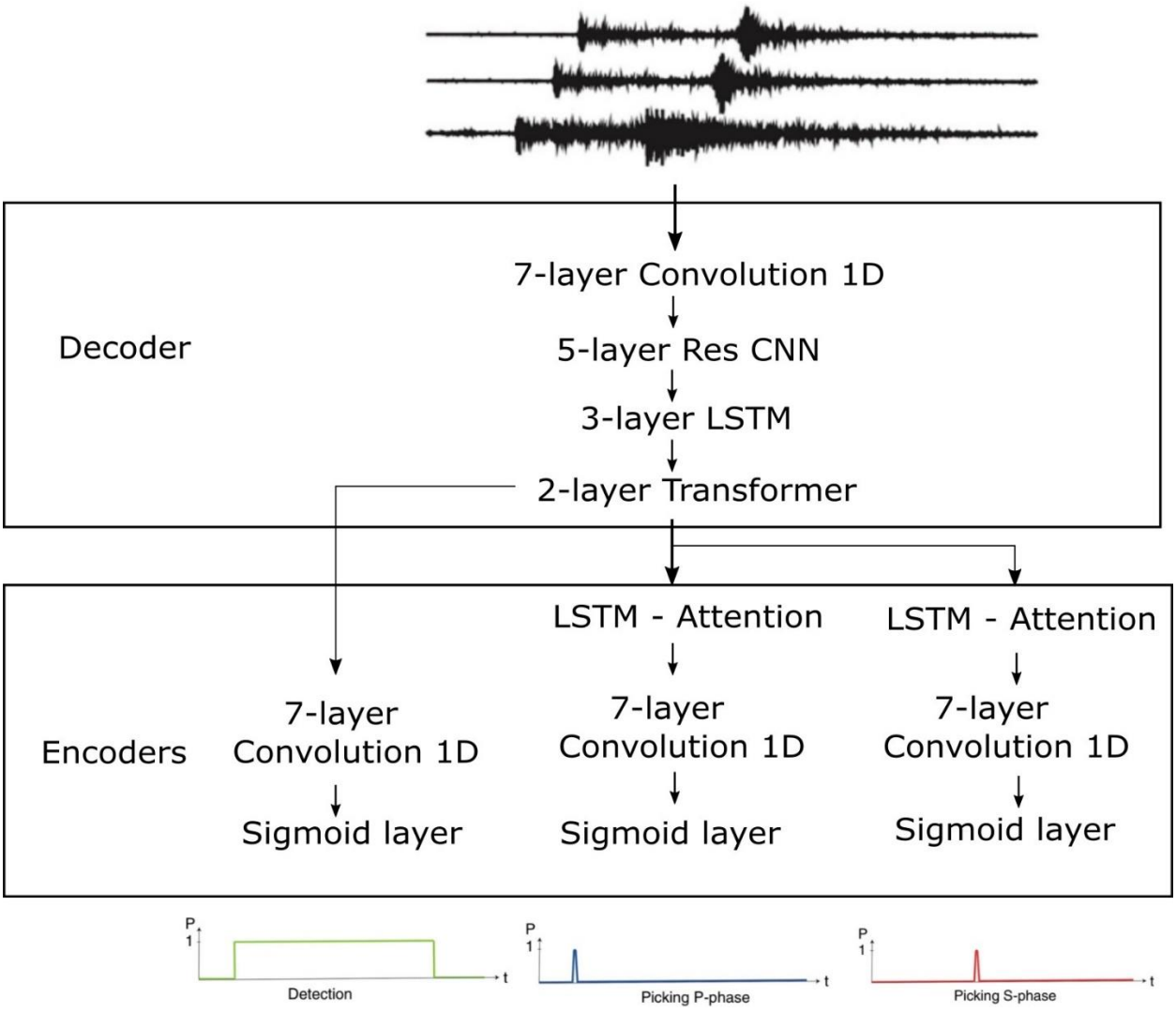

Figure 2. Simplified the network structure of the EQT model; explanation of the network structure is described in the text.

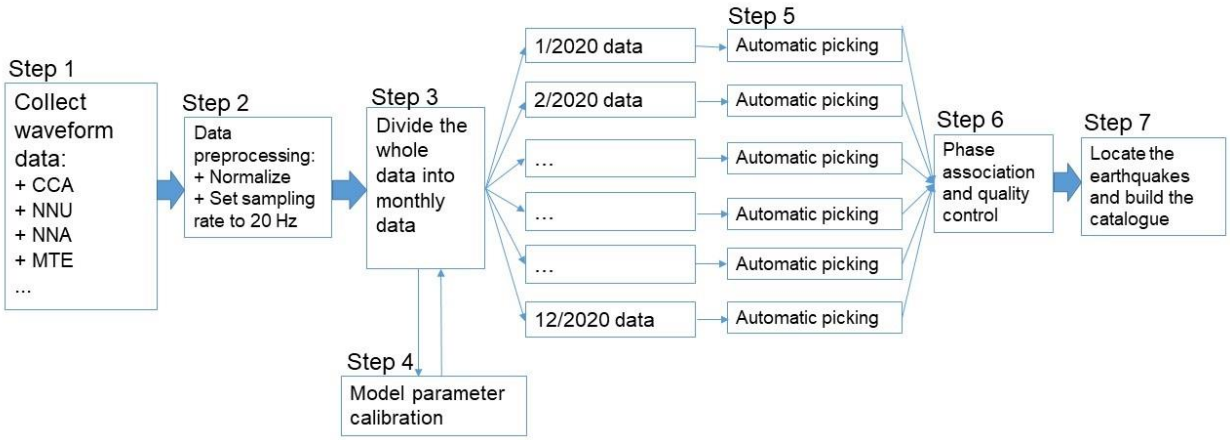

Figure 3. Data processing workflow to apply the phase picker to Muong Te seismic data.

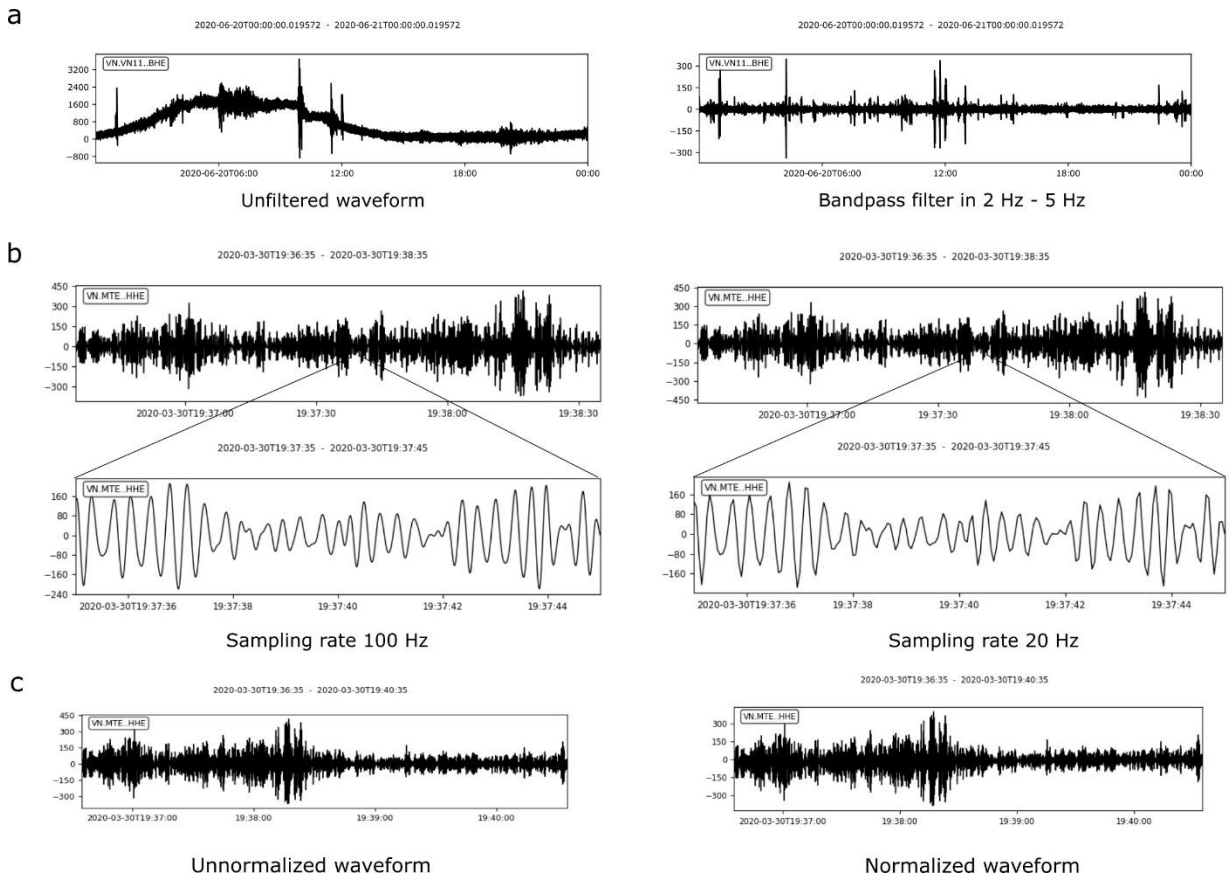

Figure 4. Data preprocessing for the raw seismic waveforms; a) bandpass filter in 2 Hz – 5 Hz; b) Downsampling rate to 20 Hz; c) normalization (detrend and demean)

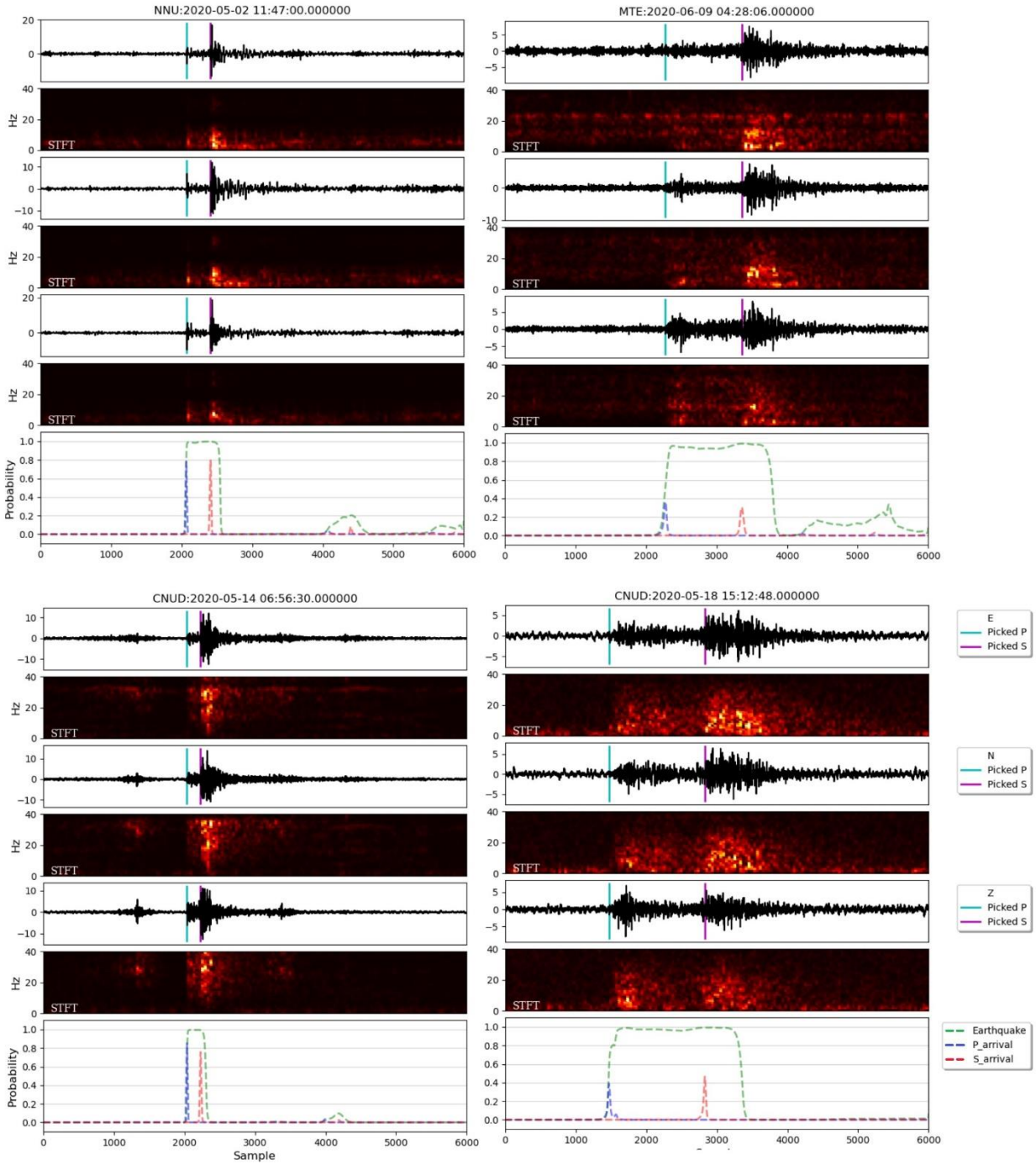

Figure 5. Examples of earthquake detection and phase picking using the EQT model. The raw waveforms are plotted without a bandpass filter. The spectrograms are the result of applying Short Time Fourier Transform (STFT) for the time-series waveform. Cyan lines mark the P arrivals while purple lines mark the S arrivals.

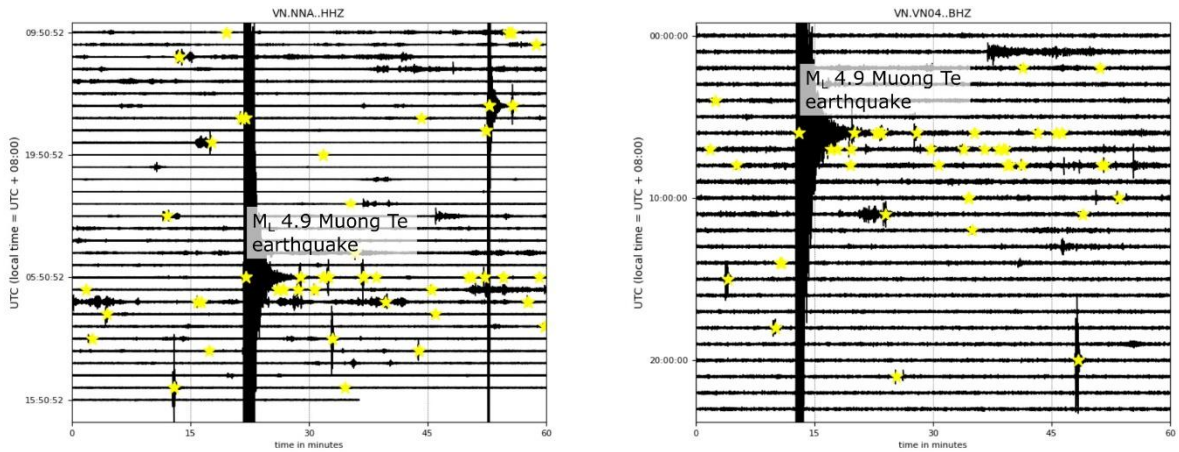

Figure 6. The Z-component seismic waveform of stations NNA and VN04 on June 16th 2020, when the M_L4.9 Muong Te earthquake occurred.

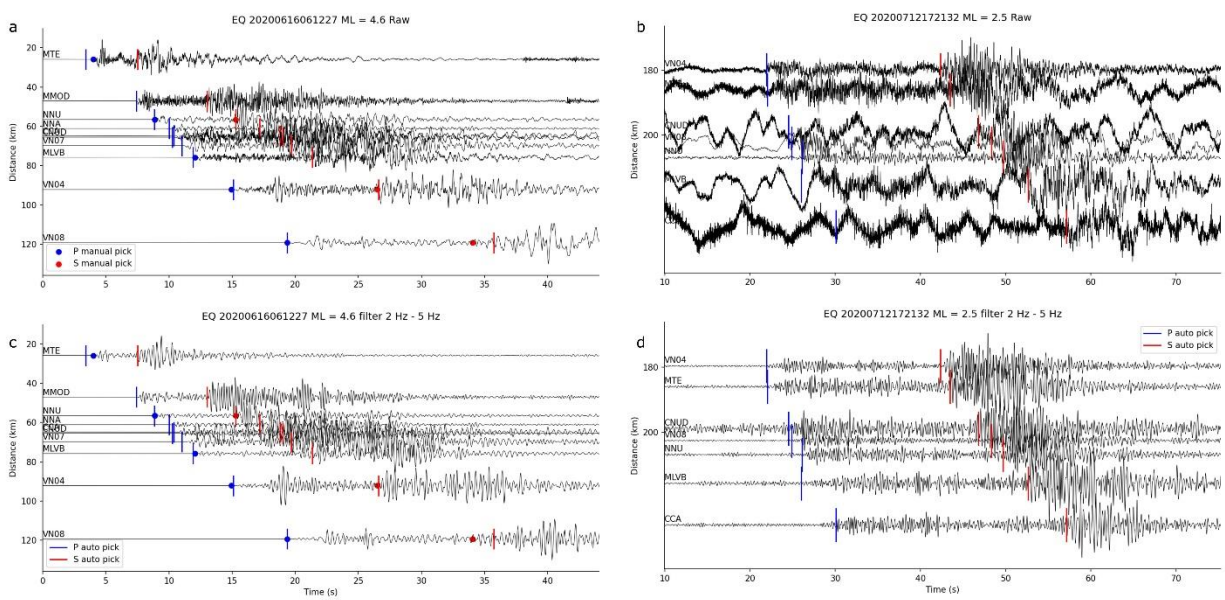

Figure 7. Examples of the phase picks for two events: the Muong Te earthquake (a, c) and an earthquake with M_L = 2.5 (b, d). Figure a) and b) show the waveforms before applying the bandpass filter, while figures c) and d) show the waveforms under the bandpass filter of 2 Hz – 5 Hz. In the first event, the manual picks are also marked with circles.

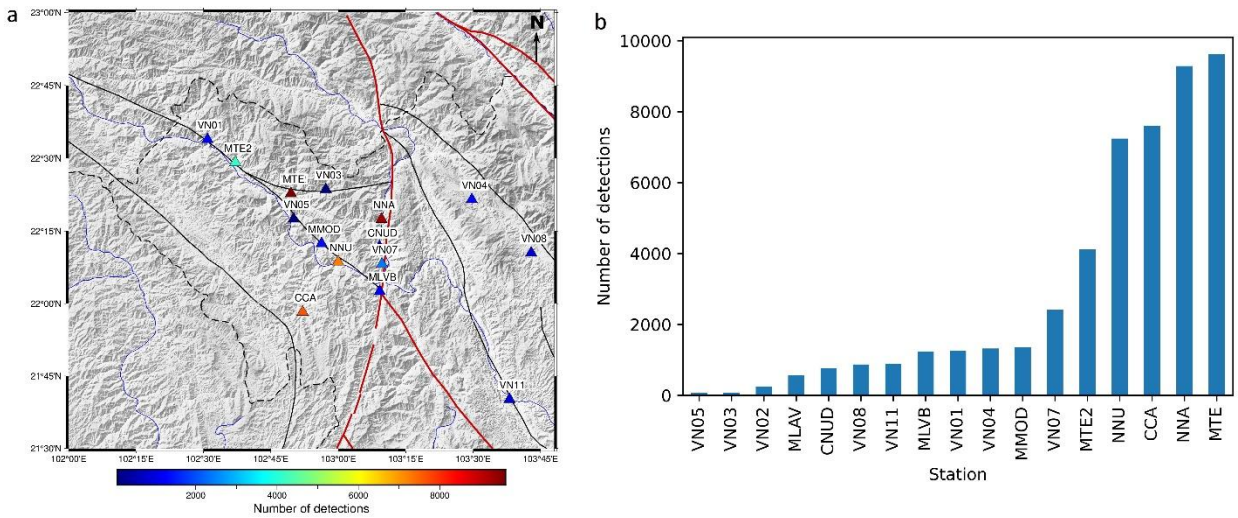

Figure 8. The number of detection for each station in the map view (a) and bar graph (b).

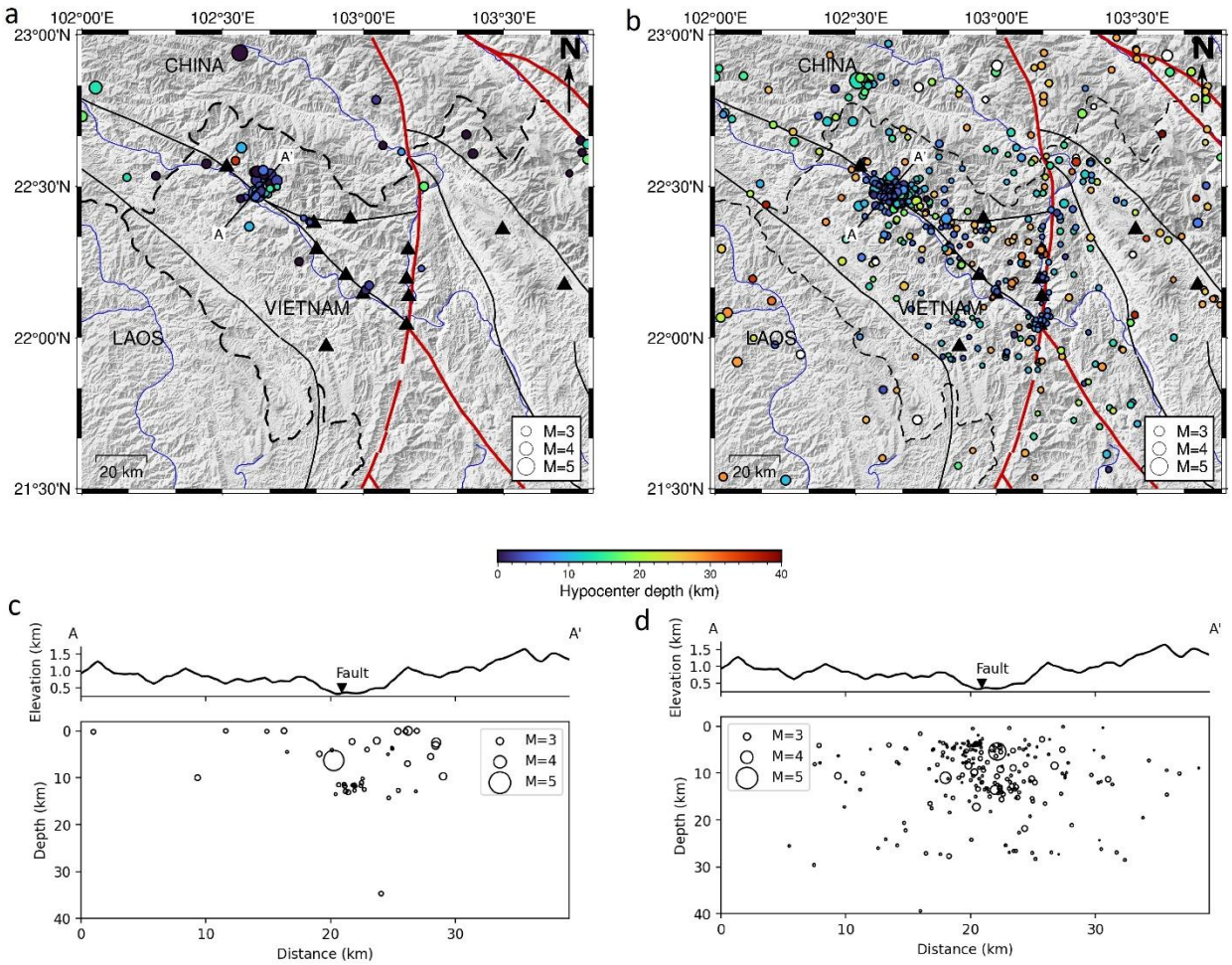

Figure 9. The earthquakes after locating process of the manual catalog MTMAN (a) and the new catalog MTEQT (b). The cross-section perpendicular to the Upstream Da River AA' in the manual catalog (c) and the new catalog (d).

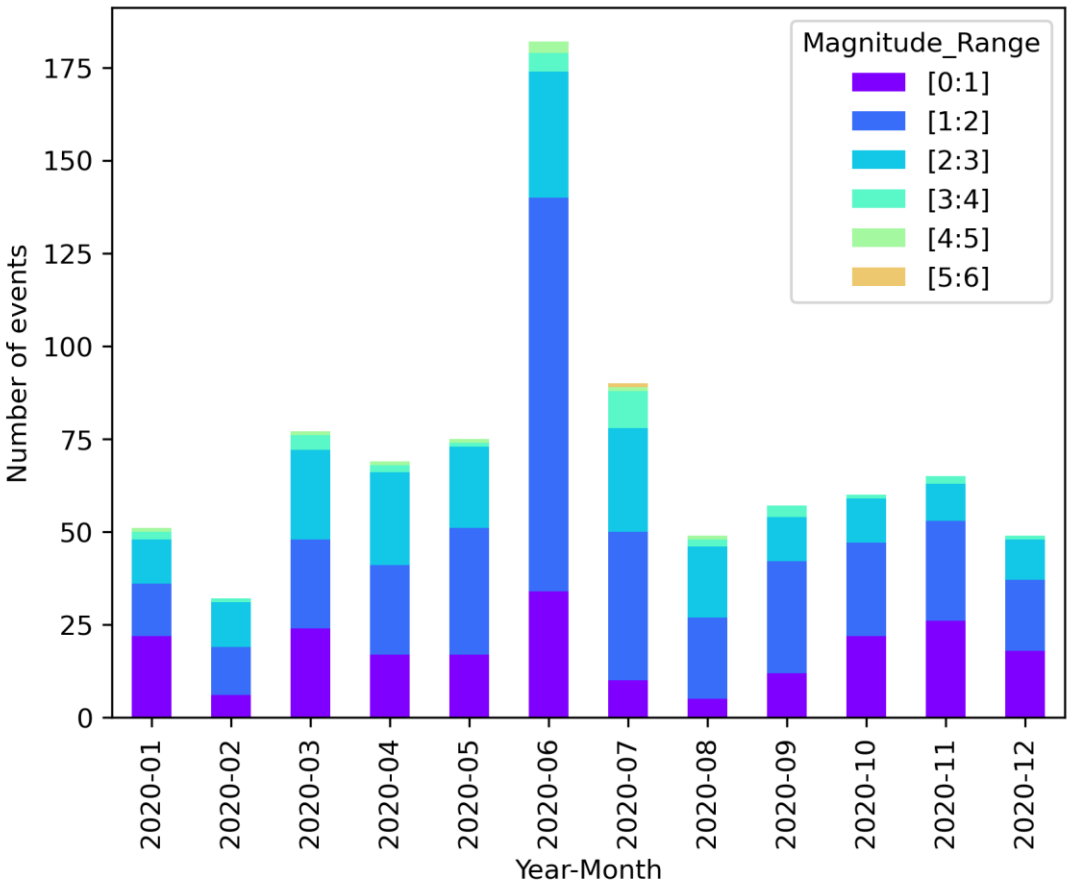

Figure 10. The number of earthquakes with their local magnitude in each month. Note the increase in the number of detected events in June 2020 and July 2020.

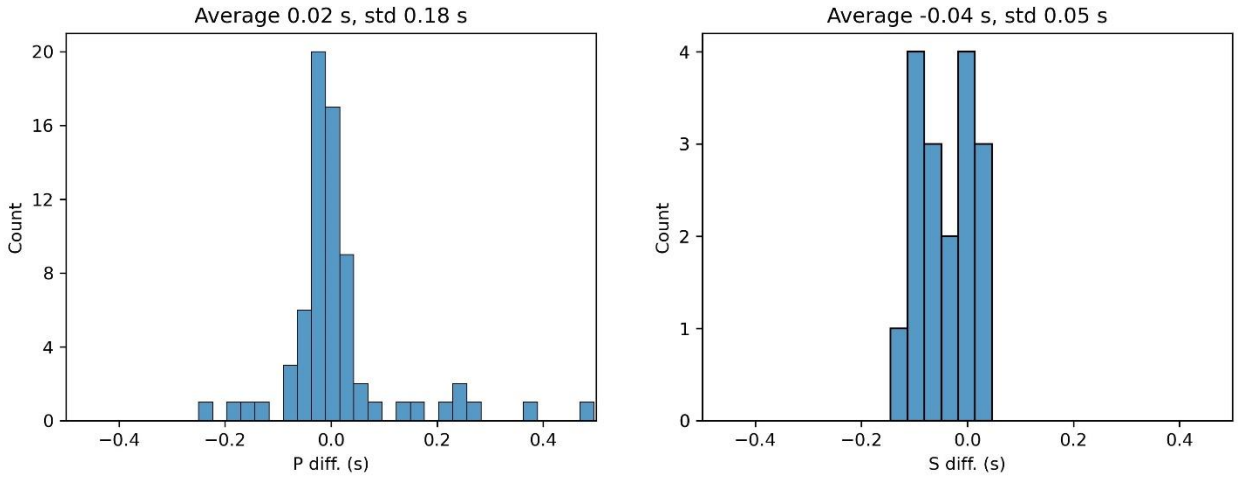

Figure 11. Histogram comparison of the phase picks between automatic catalog MTEQT and manual catalog MTMAN. The x-axis shows the time difference between automatic picking and manual picking. The positive value means the picking by EQT is later than the manual picking and vice versa.

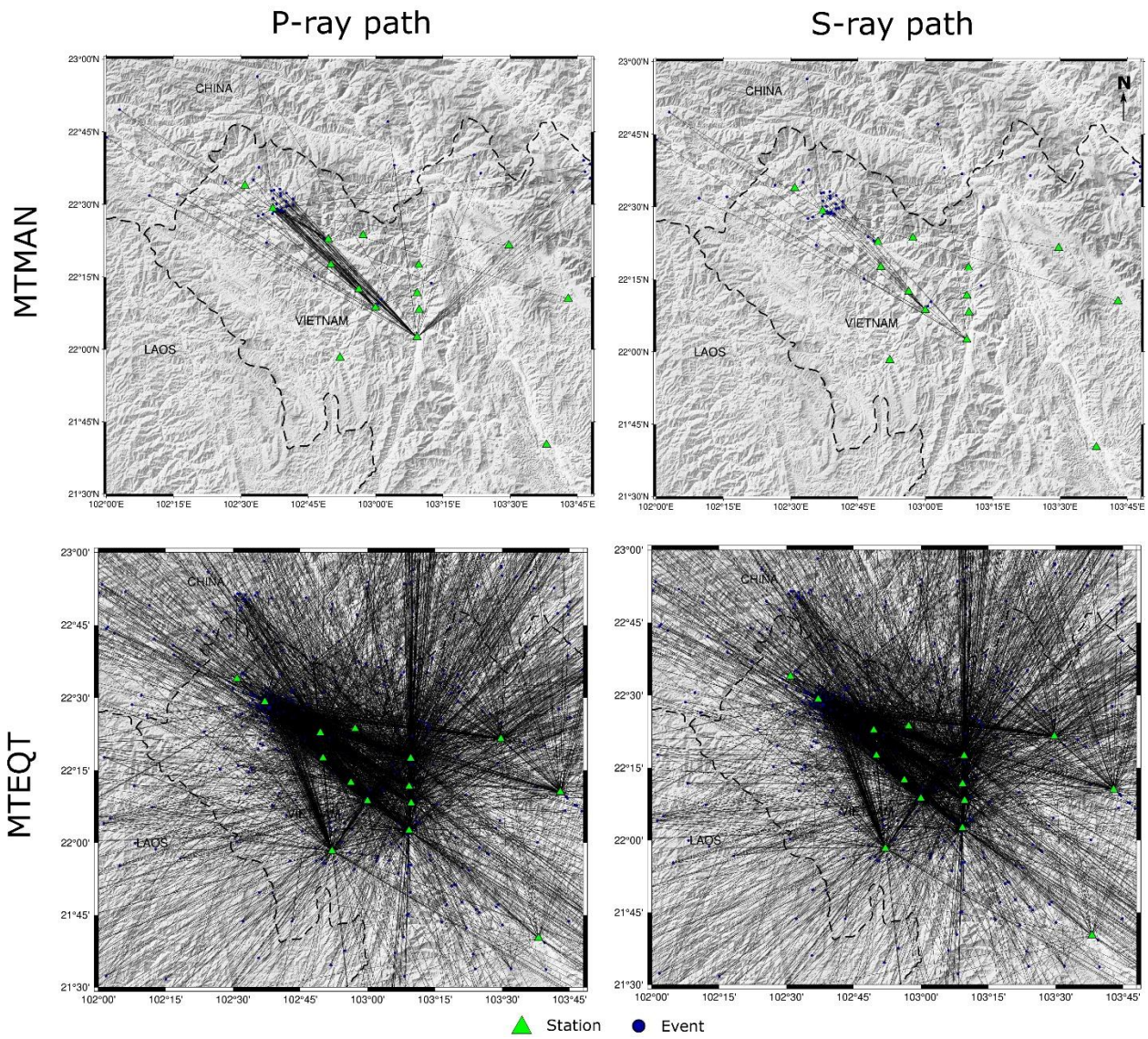

Figure 12. Crossing ray paths of the P- and S-wave from the two catalogs. Note the significant improvement of the ray paths in the automatic catalog compare MTEQT to the manual catalog MTMAN.

TABLES

Table 1. List of the seismic stations used in this study

Number	Station name	Seismometer type	Latitude (degree)	Longitude (degree)	Elevation (m)
1	CCA	Broadband	21.971	102.868	435
2	CNUD	Short period	22.194	103.154	237
3	MLAV	Short period	22.042	103.154	232
4	MLVB	Broadband	22.042	103.154	232
5	MMOD	Short period	22.207	102.938	395
6	MTE	Broadband	22.379	102.825	349
7	MTE2	Broadband	22.486	102.618	244
8	NNA	Broadband	22.291	103.160	281
9	NNU	Broadband	22.144	103.000	330
10	VN01	Broadband	22.565	102.515	373
11	VN02	Broadband	22.379	102.824	329
12	VN03	Broadband	22.393	102.954	544
13	VN04	Broadband	22.358	103.495	755
14	VN05	Broadband	22.292	102.834	38
15	VN07	Broadband	22.136	103.162	751
16	VN08	Broadband	22.175	103.715	499
17	VN11	Broadband	21.670	103.635	231

Table 2. Final model parameters of the EQT picker

Parameters	Value
Overlap	0.2
Detection threshold	0.1
P pick threshold	0.2
S pick threshold	0.2

References

Allen, R.V., 1978. Automatic earthquake recognition and timing from single traces. Bulletin of the seismological society of America 68, 1521-1532.

Baer, M., Kradolfer, U., 1987. An automatic phase picker for local and teleseismic events. Bulletin of the Seismological Society of America 77, 1437-1445.

Baillard, C., Crawford, W.C., Ballu, V., Hibert, C., Mangeney, A., 2014. An automatic kurtosis-based P-and S-phase picker designed for local seismic networks. Bulletin of the Seismological Society of America 104, 394-409.

Brodsky, E., E., 2019. The importance of studying small earthquakes. *Science*, 364 (6442), 736-737, DOI: 10.1126/science.aax2490.

Cichowicz, A., 1993. An automatic S-phase picker. Bulletin of the Seismological Society of America 83, 180-189.

Havskov, J., Ottemoller, L., 1999. SEISAN earthquake analysis software. Seismological Research Letters 70, 532-534.

Hochreiter, S., Schmidhuber, J., 1997. Long short-term memory. Neural computation 9, 1735-1780.

Hutchinson, J., Lee, R., Bradley, B., Van Houtte, C., Kaiser, A., Wotherspoon, L., 2021. Development and implications of an expanded national earthquake catalogue for New Zealand.

Hutton, L., Boore, D.M., 1987. The ML scale in southern California. Bulletin of the Seismological Society of America 77, 2074-2094.

Klein, F.W., 2002. User's guide to HYPOINVERSE-2000, a Fortran program to solve for earthquake locations and magnitudes. US Geological Survey.

Kong, Q., Trugman, D.T., Ross, Z.E., Bianco, M.J., Meade, B.J., Gerstoft, P., 2019. Machine learning in seismology: Turning data into insights. Seismological Research Letters 90, 3-14.

LeCun, Y., Bengio, Y., 1995. Convolutional networks for images, speech, and time series. The handbook of brain theory and neural networks 3361, 1995.

Lee, W.H.K., Lahr, J.C., 1972. HYPO71: A computer program for determining hypocenter, magnitude, and first motion pattern of local earthquakes. US Department of the Interior, Geological Survey, National Center for ….

Liberty, L., Mikesell, T.D., Wilbur, S., 2021. Data Analysis of the 2020 Central Idaho Mainshock-Aftershock Sequence. Idaho National Lab.(INL), Idaho Falls, ID (United States).

Liu, M., Zhang, M., Zhu, W., Ellsworth, W.L., Li, H., 2020. Rapid Characterization of the July 2019 Ridgecrest, California, Earthquake Sequence From Raw Seismic Data Using Machine-Learning Phase Picker. Geophysical Research Letters 47, e2019GL086189.

Lomax, A., Michelini, A., Curtis, A., Meyers, R., 2009. Earthquake location, direct, global-search methods. Encyclopedia of complexity and systems science 5, 2449-2473.

Mousavi, S.M., Ellsworth, W.L., Zhu, W., Chuang, L.Y., Beroza, G.C., 2020. Earthquake transformer—an attentive deep-learning model for simultaneous earthquake detection and phase picking. Nature communications 11, 1-12.

Mousavi, S.M., Sheng, Y., Zhu, W., Beroza, G.C., 2019. STanford EArthquake Dataset (STEAD): A global data set of seismic signals for AI. IEEE Access 7, 179464-179476.

Münchmeyer, J., Woollam, J., Rietbrock, A., Tilmann, F., Lange, D., Bornstein, T., Diehl, T., Giunchi, C., Haslinger, F., Jozinović, D., 2021. Which picker fits my data? A quantitative evaluation of deep learning based seismic pickers. arXiv preprint arXiv:2110.13671.

Nguyen, H.P., Pham, T.T., Nguyen, T.N., 2019. Investigation of long-term and short-term seismicity in Vietnam. *Journal of Seismology* 23, 951-966.

Ross, Z.E., Meier, M.A., Hauksson, E., Heaton, T.H., 2018. Generalized seismic phase detection with deep learning. Bulletin of the Seismological Society of America 108, 2894-2901.

Ross, Z. E., D. T. Trugman, E. Hauksson, and P. M. Shearer, 2019. Searching for hidden earthquakes in Southern California, *Science*, 364, 767-771, doi: 10.1126/science.aaw6888.

Saragiotis, C.D., Hadjileontiadis, L.J., Panas, S.M., 2002. PAI-S/K: A robust automatic seismic P phase arrival identification scheme. IEEE Transactions on Geoscience and Remote Sensing 40, 1395-1404.

Sleeman, R., Van Eck, T., 1999. Robust automatic P-phase picking: an on-line implementation in the analysis of broadband seismogram recordings. Physics of the Earth and Planetary Interiors 113, 265-275.

Trnkoczy, A., 2009. Understanding and parameter setting of STA/LTA trigger algorithm, New Manual of Seismological Observatory Practice (NMSOP). Deutsches GeoForschungsZentrum GFZ, pp. 1-20.

Trugman, D.T., Shearer, P.M., 2017. GrowClust: A hierarchical clustering algorithm for relative earthquake relocation, with application to the Spanish Springs and Sheldon, Nevada, earthquake sequences. Seismological Research Letters 88, 379-391.

Vaswani, A., Shazeer, N., Parmar, N., Uszkoreit, J., Jones, L., Gomez, A.N., Kaiser, Ł., Polosukhin, I., 2017. Attention is all you need, Advances in neural information processing systems, pp. 5998-6008.

Waldhauser, F., 2001. hypoDD--A program to compute double-difference hypocenter locations.

Waldhauser, F., Schaff, D.P., 2008. Large-scale relocation of two decades of Northern California seismicity using cross-correlation and double-difference methods. Journal of Geophysical Research: Solid Earth 113.

Wang, J., Li, T., Gu, Y.J., Schultz, R., Yusifbayov, J., Zhang, M., 2020. Sequential Fault Reactivation and Secondary Triggering in the March 2019 Red Deer Induced Earthquake Swarm. Geophysical Research Letters 47, e2020GL090219.

Wiszniowski, J., Plesiewicz, B., Lizurek, G., 2021. Machine learning applied to anthropogenic seismic events detection in Lai Chau reservoir area, Vietnam. Computers & Geosciences 146, 104628.

Xiao, Z., Wang, J., Liu, C., Li, J., Zhao, L., Yao, Z., 2021. Siamese Earthquake Transformer: A pair-input deep-learning model for earthquake detection and phase picking on a seismic array. Journal of Geophysical Research: Solid Earth 126, e2020JB021444.

Zhao, D., 2015. Multiscale seismic tomography. Springer.

Zhou, L., Zhao, C., Zhang, M., Xu, L., Cui, R., Zhao, C., Duan, M., Luo, J., 2021. Machine-learning-based earthquake locations reveal the seismogenesis of the 2020 Mw 5.0 Qiaojia, Yunnan earthquake. Geophysical Journal International 228, 1637-1647.

Zhu, W., Beroza, G.C., 2019. PhaseNet: a deep-neural-network-based seismic arrival-time picking method. Geophysical Journal International 216, 261-273.